

Measurement of statistical nuclear spin polarization in a nanoscale GaAs sample

Fei Xue, D. P. Weber, P. Peddibhotla, and M. Poggio

*Department of Physics, University of Basel,
Klingelbergstrasse 82, 4056 Basel, Switzerland*

(Dated: October 11, 2024)

Abstract

Magnetic resonance force microscopy is used to measure the statistical polarization of quadrupolar nuclear spins in a sub-micrometer ($0.6 \mu\text{m}^3$) particle of GaAs. The crystalline sample is cut out of a GaAs wafer and attached to a micro-mechanical cantilever force sensor using a focused ion beam technique. Experiments demonstrate a sensitivity to an ensemble of order 10^6 nuclear spins – a number nearly small enough that random spin fluctuations, rather than Boltzmann polarization, dominate its dynamics. This sensitivity corresponds to that required to detect a volume of GaAs smaller than $(100 \text{ nm})^3$ and represents an important first step toward 3D magnetic resonance imaging of III-V structures on the nanometer-scale.

PACS numbers: 76.70.-r, 05.40.-a, 68.37.Rt, 85.85+j

Recent years have seen the development of a wide range of semi-conducting nanostructures including quantum wells (QWs), nanowires (NWs), and quantum dots (QDs). Researchers have devoted particular attention to making devices from III-V materials such as GaAs, whose high electron mobility and direct band gap make it a critical component of today's semiconductor technology. III-V systems are extremely versatile in large part due to techniques such as molecular beam epitaxy (MBE) and metal-organic chemical vapor deposition (MOCVD), which enable the growth of complex heterostructures with nearly perfect crystalline interfaces. As a result, applications range from integrated circuits operating at microwave frequencies to light-emitting and laser diodes to quantum structures used for basic research.

While a variety of techniques exist to characterize and image these nanostructures, including scanning electron microscopy (SEM), tunneling electron microscopy (TEM), and x-ray crystallography, so far it has been impossible to measure single nano-structures using magnetic resonance imaging (MRI). In larger structures, MRI is a powerful technique allowing for the three-dimensional (3D), sub-surface imaging of the density of particular nuclear magnetic moments. However, conventional nuclear magnetic resonance (NMR) techniques, in which the spin signal is detected by an inductive pick-up coil, are limited to detection volumes of several μm on a side or larger [1]. A net polarization of at least 10^{12} nuclear spins is typically needed to generate a detectable signal; nanometer-scale samples simply do not contain enough spins to be detected. In the past few years, a more sensitive force-detected version of MRI has been demonstrated on nanometer-scale samples [2]. Using magnetic resonance force microscopy (MRFM) to measure the statistical polarization of spin-1/2 ^1H , Degen et al. made 3D images of single virus particles with a resolution better than 10 nm [3].

Here we take a step toward applying this technique to quadrupolar (spin-3/2) nuclei, specifically Ga and As, in a nanometer-scale particle. We demonstrate the detection of statistical polarizations of ^{69}Ga , ^{71}Ga , and ^{75}As in a $0.6 \mu\text{m}^3$ particle of crystalline GaAs. The mechanical detection of NMR in GaAs was first demonstrated in 2002 by Verhagen et al. and Thurber et al. [4, 5]. The smallest reported detection volume of $600 \mu\text{m}^3$ contained more than 10^{12} nuclear moments [6]. In 2004 Garner et al. reported forced-detected NMR signal from 10^{10} moments in a GaAs wafer with the smallest detectable ensemble estimated at 7.1×10^8 moments [7]. Those experiments measured either the thermal equilibrium polarization

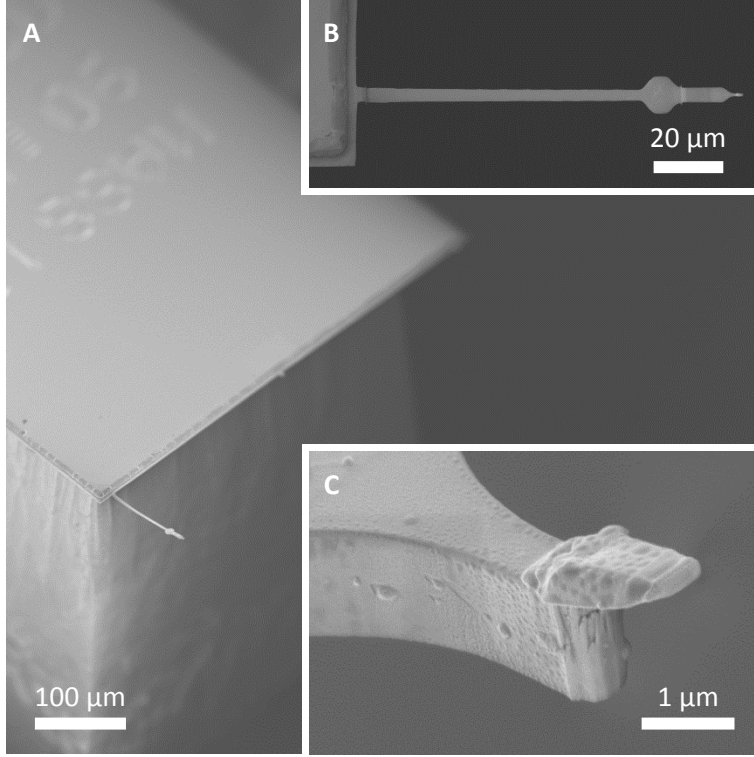


FIG. 1: SEM micrograph of the Si cantilever with a GaAs sample attached. (A) shows the cantilever protruding from a Si chip. (B) clarifies the geometry showing the paddle and mass-loaded end of the cantilever, and (C) is a detailed view of the tip of the mass-loaded cantilever with the GaAs sample attached.

or an optically enhanced polarization of Ga and As spin ensembles. Our experiment has a detection volume of about $0.03 \mu\text{m}^3 \approx (300 \text{ nm})^3$ and we estimate that the smallest detectable ensemble contains around 10^6 nuclear moments, representing a volume of GaAs smaller than $(100 \text{ nm})^3$. Such a volume is far too tiny to detect via conventional, inductively-detected magnetic resonance. Furthermore, the number of spins in the ensemble is nearly small enough that its polarization is dominated by statistical fluctuations.

Conventional magnetic resonance signals originate from the mean polarization of nuclear spins in an external magnetic field – the so-called Boltzmann polarization. Although this polarization is quite small, it dominates the spin signal for large ensembles of nuclear spins. As the size of the spin ensemble decreases, the amplitude of the polarization fluctuations eventually exceeds the mean polarization [8]. This variance, sometimes called the statistical polarization, then becomes a more useful signal for MRI than the mean polarization.

Statistical polarization arises from the incomplete cancellation of randomly oriented spins. For any given direction, the net polarization can be either positive or negative and will fluctuate on a time scale that depends on the flip rate of the spins. Several MRFM experiments have detected statistical polarizations of nuclear spins [9–14] and demonstrated the use of statistical polarization for nanometer-scale nuclear MRI [3, 15].

In order to understand the regimes in which either Boltzmann or statistical polarization is important, consider an ensemble of N spins with spin quantum number I . The Hamiltonian of a single spin in the presence of a magnetic field B along the z -direction is $\hat{H} = -\hat{\mu}_z B = -\hbar\gamma B \hat{I}_z$ where $\hat{\mu}_z$ is the magnetic dipole moment operator in the z -direction, \hbar is Planck's constant, γ is the gyromagnetic ratio, and \hat{I}_z is the nuclear spin angular momentum operator in the z -direction. Statistical mechanics predicts the equilibrium distribution at a temperature T to be a Boltzmann distribution. The partition function $Z = \text{Tr}\{e^{-\frac{\hat{H}}{k_B T}}\}$ contains all the information about the nuclear spin polarization in the system [16]. The density matrix $\hat{\rho} = \frac{1}{Z}e^{-\frac{\hat{H}}{k_B T}}$ of the spin system can be used to compute the mean $M_z = N \text{Tr}\{\hat{\mu}_z \hat{\rho}\}$ and the variance $\sigma_{M_z}^2 = N(\text{Tr}\{\hat{\mu}_z^2 \hat{\rho}\} - (\text{Tr}\{\hat{\mu}_z \hat{\rho}\})^2)$ of the ensemble's magnetization in the z -direction. Even at cryogenic temperatures ($T \sim 1$ K) and high magnetic fields ($B \sim 10$ T), $\hbar\gamma B \ll k_B T$. Therefore, keeping terms only up to first order in $\frac{\hbar\gamma B}{k_B T}$, we find:

$$M_z = N \frac{I(I+1)}{3} \hbar\gamma \left(\frac{\hbar\gamma B}{k_B T} \right), \quad (1)$$

$$\sigma_{M_z}^2 = N \frac{I(I+1)}{3} (\hbar\gamma)^2. \quad (2)$$

Since $N\hbar\gamma I$ corresponds to 100% spin polarization, one can define the statistical nuclear polarization as $SNP = \frac{\sigma_{M_z}}{N\hbar\gamma I} = \sqrt{\frac{I+1}{3I} \frac{1}{N}}$ and the Boltzmann nuclear polarization as $BNP = \frac{M_z}{N\hbar\gamma I} = \frac{I+1}{3} \frac{\hbar\gamma B}{k_B T}$. Statistical polarization dominates the system ($SNP > BNP$) when the number of spins in an ensemble is less than the critical number,

$$N_c = \frac{3}{I(I+1)} \left(\frac{k_B T}{\hbar\gamma B} \right)^2. \quad (3)$$

Equivalently, for a material with nuclear spin density ρ_I one can define a critical volume $V_c = \frac{N_c}{\rho_I}$. For volumes smaller than V_c , magnetic resonance experiments should be designed to detect SNP rather than BNP .

We use MRFM to measure the presence of a particular nuclear isotope by cyclically inverting its statistical spin polarization [15]. In a constant magnetic field $\mathbf{B} = B \hat{z}$, the

frequency of a transverse RF magnetic field B_1 is swept through the nuclear resonance condition, $f_{\text{RF}} = \frac{\gamma}{2\pi}B$. If done adiabatically, this sweep induces the nuclear spins to invert – a process known as adiabatic rapid passage. In the strong spatial magnetic field gradient near a magnetic tip, these inversions produce a time-dependent force. This force is in turn detected as the displacement of an ultrasensitive cantilever. Our MRFM experiment is carried out in a sample-on-cantilever configuration in which the sample is affixed to the end of a single-crystal Si cantilever [17]. We arrange the cantilever in a “pendulum” geometry such that the sample is positioned above a FeCo magnetic tip. The magnetic tip, which is mounted on a separate chip, is patterned on top of an Au microwire, which acts as an RF magnetic field source [10].

The cantilever measures $120 \mu\text{m} \times 4 \mu\text{m} \times 0.1 \mu\text{m}$ (Fig. 1) and, loaded with the GaAs sample, has a mechanical resonance frequency $f_c = \omega_c/(2\pi) = 3.7 \text{ kHz}$ and an intrinsic quality factor $Q = 4.0 \times 10^4$ at $T = 1 \text{ K}$. By measuring the cantilever’s thermal motion, we determine its effective spring constant to be $k = 85 \mu\text{N/m}$. The MRFM apparatus is isolated from vibrational noise and is mounted in a vacuum chamber with a pressure below 10^{-6} mbar at the bottom of a ^3He cryostat. The motion of the lever is detected using 100 nW of 1550 nm laser light focused onto a 12 μm -wide paddle and reflected back into an optical fiber interferometer. The microwire used to produce the transverse RF magnetic field is 2.5 μm -long, 1 μm -wide, and 0.2 μm -thick. The FeCo tip is shaped like a bar (top width: 270 nm, bottom width: 510 nm, length: 1.2 μm , height: 265 nm; see supplementary material), sits on top of the microwire, and produces a spatially dependent field $\mathbf{B}_{\text{tip}}(\vec{r})$. To make sure that the FeCo tip is fully magnetized along the z -direction, an external magnetic field $B = 2.65 \text{ T}$ is applied. During measurements the distance between the magnetic tip and the closest point on the sample is less than 200 nm such that the static magnetic field gradient $\frac{\partial B_{\text{total}}}{\partial x}$ relevant to MRFM is 10^5 T/m or larger, where $\mathbf{B}_{\text{total}} = \mathbf{B} + \mathbf{B}_{\text{tip}}$ and x is the direction of cantilever oscillation. Interactions between the magnetic tip and the sample at such small gaps, known as non-contact friction, lead to mechanical dissipation in the cantilever [18, 19]. In our experiments, these effects reduce the quality factor Q of the cantilever to 1.0×10^4 . In addition, we damp Q down to ~ 500 in order to increase the bandwidth of our force detection without sacrificing force sensitivity [20].

If the rate of the RF frequency sweeps used to invert the nuclear spins is slow enough and the amplitude of B_1 large enough, the initial population distribution among the nuclear spin

energy levels is completely inverted. As a result, the net magnetization is made to flip along the z -direction. For spin-1/2 nuclei, the criterion for adiabatic inversion is given by $\alpha = 2\pi\gamma^2 B_1^2 / (\omega_c \Omega_{\text{RF}}) \gg 1$, where $\Omega_{\text{RF}} / (2\pi)$ is the amplitude of the frequency modulation around the carrier frequency of the transverse RF field B_1 [16]. The criterion for quadrupolar nuclei, in general, is more complex [21]. However, a complete inversion of the initial population distribution over the quadrupolar energy levels can be achieved in the limit of both $\alpha \gg 1$ and $\beta = \gamma B_1 / \Omega_Q \gg 1$, where $\Omega_Q / (2\pi)$ is the quadrupolar frequency. The specific form of the frequency sweeps used here is designed to meet these conditions throughout and follows the form used in Ref. [10]. Therefore, by sweeping f_{RF} at a frequency $2f_c$, we are able to modulate the spin polarization at f_c . The resulting spin inversions produce a force that drives the cantilever at its resonance frequency. An ensemble of spins with a statistical variance in its z -magnetization $\sigma_{M_z}^2$ produces a force on the cantilever with variance $\sigma_F^2 = \sigma_{M_z}^2 \left(\frac{\partial B_{\text{total}}}{\partial x} \right)^2$, for the value of $\frac{\partial B_{\text{total}}}{\partial x}$ at the position of the spin ensemble. The correlation time of σ_F^2 is limited by the relaxation rate of the spins in the rotating frame. We determine σ_F^2 by measuring the variance of the cantilever's oscillations on resonance and using our knowledge of the lever spring constant k .

Here we study a sub-micron sized particle cut from the surface of a GaAs wafer. The GaAs sample is affixed to the cantilever tip using a focused ion beam (FIB) technique. First, a thin layer of Pt is deposited over a small area of a GaAs wafer to protect the sample from potential ion damage. Then, a lamella measuring $3 \mu\text{m} \times 2 \mu\text{m} \times 0.3 \mu\text{m}$ is cut out from this area of the wafer (see supplementary material). Next, the lamella is welded with Pt to a nearby micro-manipulator and transferred to the tip of an ultrasensitive Si cantilever. Finally, the particle is Pt-welded to the cantilever tip and cut to its final dimensions: $2.4 \mu\text{m} \times 0.8 \mu\text{m} \times 0.3 \mu\text{m} = 0.6 \mu\text{m}^3$ (Fig. 1). The side of the sample which formerly was part of the wafer surface is oriented such that it faces away from the cantilever. A roughly 200 nm-thick layer of the original Pt protection layer remains on this surface of the particle.

MRFM signal measured from this GaAs particle at $B = 2.65$ T and temperature $T = 1$ K is plotted as a function of the RF carrier frequency in Fig. 2. Resonances from all three isotopes (^{69}Ga , ^{71}Ga , and ^{75}As) in GaAs are visible. In addition, a strong ^1H resonance appears in the spectrum due to the thin layer of adsorbed hydrocarbons and water that coats surfaces which have been exposed to ordinary laboratory air [3, 15]. Though this layer is typically on the order of 1 nm thick, it produces a stronger signature than the quadrupolar

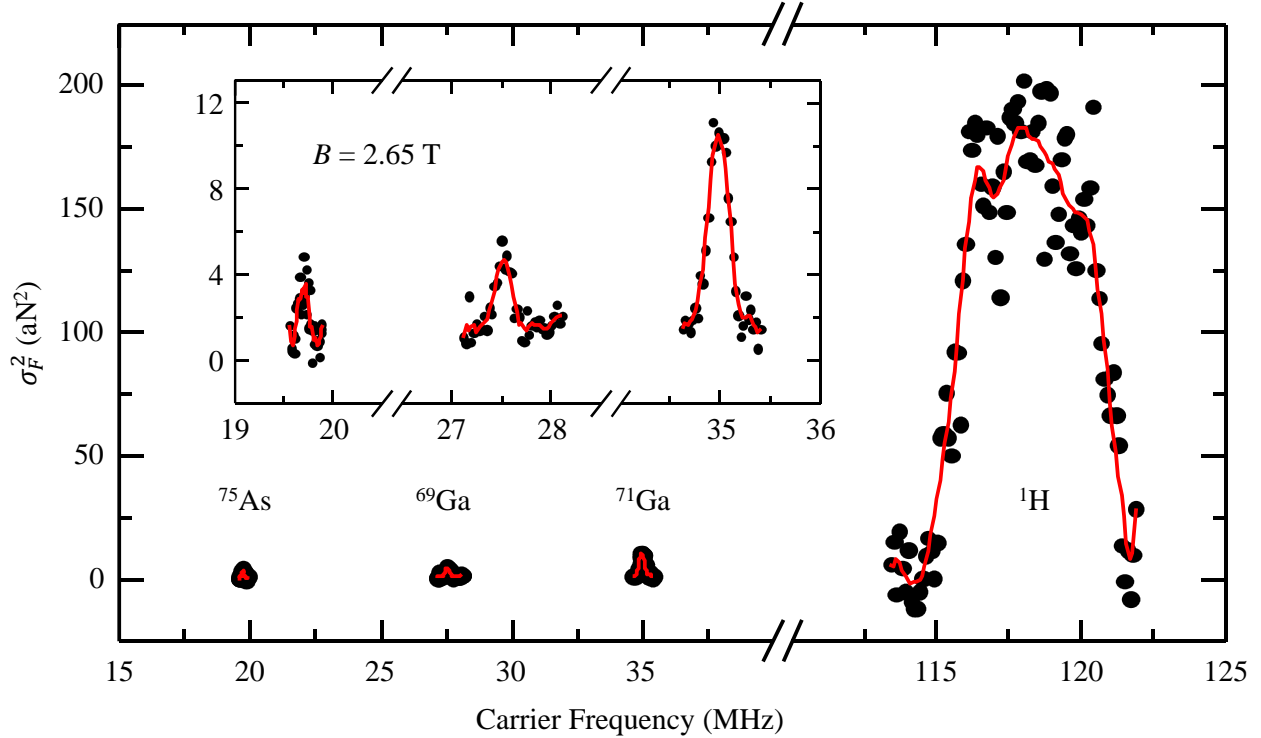


FIG. 2: MRFM signal from the statistical polarization of ^1H , ^{69}Ga , ^{71}Ga , and ^{75}As . Black dots show the resonant force variance σ_F^2 as a function of the carrier frequency for RF magnetic field from the four different isotopes. Solid red lines represent adjacent-averaging of the data. Inset is a zoomed-in view of the spin-3/2 nuclear resonances: ^{69}Ga , ^{71}Ga , and ^{75}As .

nuclei in the GaAs particle for three reasons. First, due to the 200 nm Pt layer covering the tip of the GaAs particle, the ^1H containing layer is 200 nm closer to the FeCo tip than any of the isotopes in GaAs. As a result, the ^1H nuclei experience about ten times higher $\frac{\partial B_{\text{total}}}{\partial x}$ than the quadrupolar isotopes – resulting in force variances 100 times larger from the same magnetization. Second, the density of ^1H in a typical hydrocarbon layer ($7 \times 10^{28} \text{ m}^{-3}$) is almost twice the density of Ga or As in GaAs ($4.2 \times 10^{28} \text{ m}^{-3}$). Finally, the magnetization variance expected from an ensemble of ^1H moments is about five times greater than that expected from an equal number of quadrupolar nuclei in GaAs.

This difference in magnetization variance is contained within the concept of receptivity. Receptivity is a value defined for the purpose of comparing the expected NMR signal magnitudes for equal numbers of different nuclear species. For MRFM of statistically polarized ensembles, we define a receptivity, $R_{\text{MRFM}} \propto \eta \gamma^2 I(I+1)$, where η is the natural abundance of a particular isotope and R_{MRFM} is normalized to 1 for ^1H . The factor η represents the

fraction of the desired isotope for a particular element. The factor $\gamma^2 I(I+1)$ is proportional to the magnetization variance expected from an ensemble of spins as defined in equation (2). This variance, multiplied by the square of the magnetic field gradient, results in the resonant force variance measured in MRFM.

On the other hand, conventional NMR collects an inductive signal due to a Boltzmann polarization. In this case, receptivity $R_{\text{conv}} \propto \eta \gamma^3 I(I+1)$ is similarly normalized to 1 for ^1H . Here η again comes from the fraction of the relevant isotope and the factor $\gamma^2 I(I+1)$ is proportional to the Boltzmann polarization as defined in equation (1). The remaining factor of γ results from the fact that conventional NMR measures the inductive response of a pick-up coil to magnetization precessing at a frequency proportional to γ [22]. As can be noted in top section of table I, MRFM receptivity scales more favorably than conventional receptivity for low- γ nuclei such as those found in GaAs.

Using the method described in Ref. [10], we also measure the magnitude of B_1 . Pulses with variable length are inserted in the adiabatic sweep waveform every 500 cantilever cycles (135 ms). The measured force variance in spin nutation experiments of ^{71}Ga is plotted in Fig. 3. The amplitude of the rotating RF magnetic field is inferred by fitting the data to a decaying sinusoid. B_1 is measured to be 16 mT within 400 nm of the magnetic tip, resulting in Rabi frequencies of 680 kHz for ^1H , 165 kHz for ^{69}Ga , 208 kHz for ^{71}Ga and 117 kHz for ^{75}As . The modulation amplitude $\Omega_{\text{RF}}/(2\pi)$ used in our frequency sweeps is 800 kHz for ^1H , 200 kHz for ^{69}Ga and ^{71}Ga , and 100 kHz for ^{75}As . In crystalline GaAs a small amount of strain due to the mounting process can result in non-zero quadrupolar frequencies Ω_Q , though their splittings are typically on the order of 10 kHz for all isotopes [24, 25]. Therefore our experiments operate in the limit of both $\alpha \gg 1$ and $\beta \gg 1$, allowing for complete adiabatic inversion of all four nuclear species.

In order to estimate the number of spins in our detection volume, we must consider the effect of the FeCo tip. Since the magnetic field near this tip is strongly inhomogeneous, there is a specific region in space at which the magnetic resonance condition is met. Only spins near these positions are adiabatically inverted and thus included in the MRFM detection volume. This so-called resonant slice is a shell-like region in space above the magnetic tip whose thickness is determined by the magnetic field gradient and the modulation amplitude of the frequency sweeps. The exact shape of the slice is determined by the magnetic field profile of the FeCo tip. We determine this profile using a method employed in other recent

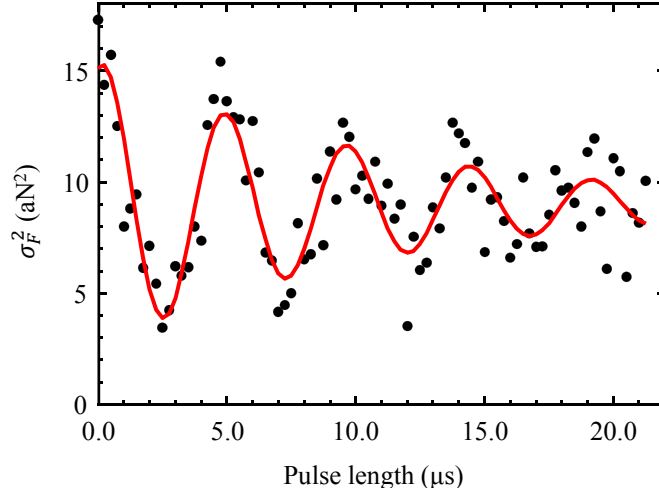


FIG. 3: Nutation measurement for ^{71}Ga at $T = 1$ K. Resonant force variance from ^{71}Ga spins is measured as a function of pulse length. A rotating RF magnetic field amplitude B_1 of 16 mT is obtained from a decaying sinusoidal fit (shown in red) to the Rabi oscillations.

MRFM experiments [3, 23]. First, we measure the width of the ^1H resonance peak for different positions of the sample relative to the FeCo tip. These data represent measurements of the local magnetic field in the vicinity of the tip.

Using these measured values, we then calibrate a magnetostatic model of the FeCo tip, whose shape is inferred from SEM images. The resulting magnetic field profile $B_{\text{total}}(\vec{r})$, allows us to determine both $\frac{\partial B_{\text{total}}}{\partial x}(\vec{r})$ and the form of the resonant slice. Since the gradient varies throughout the resonant slice, equal volumes of spins at different positions in the slice contribute different forces to the final signal. In order to estimate the number of spins contributing to a given force signal, a full spatial integration must be carried out over the intersection of the resonant slice and the sample.

We therefore construct a simple theory based on $B_{\text{total}}(\vec{r})$ and an effective field model for adiabatic rapid passage in the manner of the appendix in Ref. [3]. Input parameters to this model include the form of the adiabatic sweeps, the mechanical characteristics of the cantilever, and the geometry of the sample. Given our approximate knowledge of the shape of the sample from SEM images (see Fig. 1), the results can only be used to make the order of magnitude estimates shown in the bottom of table I. Nevertheless, the model reproduces the size and shape of the resonances shown in Fig. 2 within the error of our parameters. Furthermore, it allows us to estimate the approximate number of spins contributing to each

	^1H	^{69}Ga	^{71}Ga	^{75}As
I	1/2	3/2	3/2	3/2
η	1.000	0.601	0.399	1.000
$\frac{\gamma}{2\pi}$ (MHz/T)	42.57	10.3	13.0	7.3
R_{MRFM}	1	0.18	0.19	0.15
R_{conv}	1	0.043	0.057	0.025
N_c ($B = 2.65$ T, $T = 1$ K)	1.4×10^5	4.7×10^5	2.9×10^5	9.3×10^5
V_c ($B = 2.65$ T, $T = 1$ K)	$(12 \text{ nm})^3$	$(33 \text{ nm})^3$	$(32 \text{ nm})^3$	$(35 \text{ nm})^3$
Sample-tip distance (nm)	70	370	370	370
Maximal $\frac{\partial B_{\text{total}}}{\partial x}$ at sample (T/m)	1.1×10^6	0.8×10^5	0.8×10^5	0.8×10^5
Averaging time (s)	120	600	600	1400
Number of detected spins	3×10^6	4×10^8	2×10^8	6×10^8
Detection volume	$(30 \text{ nm})^3$	$(310 \text{ nm})^3$	$(290 \text{ nm})^3$	$(300 \text{ nm})^3$
Spin sensitivity	4×10^4	2×10^6	1×10^6	4×10^6
Volume sensitivity	$(8 \text{ nm})^3$	$(50 \text{ nm})^3$	$(50 \text{ nm})^3$	$(60 \text{ nm})^3$

TABLE I: Properties and Estimates

signal, and thus the size of the detection volume.

In addition, we can calculate the sensitivity of each experiment in terms of the smallest detectable ensemble of spins. This number can be estimated by solving for the size of the spin ensemble required to produce a force equivalent to a SNR of 1 at the position of maximal $\frac{\partial B_{\text{total}}}{\partial x}$. This sensitivity represents the minimum number of nuclear moments (or the minimum volume of material) required to produce a signal detectable by each experiment.

The variation in sensitivity between experiments is due to the different magnetic moment and density of each isotope, the slightly different conditions of each experiment, and differences in measurement time. The sensitivity of these measurements improves proportionally to the square-root of the measurement time. In the case of the ^1H layer on the surface of the sample, the experiment is sensitive to volumes well within the regime where statistical polarization dominates after only 2 min of averaging. For the quadrupolar nuclei within the GaAs particle, 10 min or more are required to become sensitive to nanometer-scale volumes, which approach – but are not yet within – the statistical regime. This reduced sensitivity is

partly due to the smaller magnetic moment of these nuclei, though it is mostly due to the thick Pt layer which forces the GaAs to be 200 nm further away from the FeCo tip than the hydrogen surface layer. The small gradients at these large tip-sample distances dramatically reduce the measurement sensitivity. Future experiments, with thinner or no Pt layer can be expected to be sensitive to GaAs volumes small enough to be within the statistical regime. Note, however, that even in this early demonstration each experiment is sensitive to volumes of GaAs smaller than $(100 \text{ nm})^3$.

The results presented here, demonstrate our ability to detect nanometer-scale volumes of Ga and As nuclei using MRFM. Given the spin sensitivity determined from our data, the detection of sub-surface III-V nanostructures such as QWs or self-assembled InAs QDs should be possible. Self-assembled InAs QDs, for example, contain 10^5 – 10^7 nuclear spins, lie 50–200 nm below the wafer surface, and could be attached to a cantilever using the FIB technique described here. Further improvements to the force sensitivity – most importantly for reducing measurement times – will be required in order to realize MRI in III-V materials with better than 100 nm resolution. The potential for sub-surface, isotopically selective imaging on the nanometer-scale in III-V materials is a particularly exciting prospect since conventional methods such as SEM and TEM lack isotopic contrast.

The authors thank Dr. Erich Müller from the Laboratory for Electron Microscopy at the Karlsruhe Institute of Technology for conducting the FIB process. We acknowledge support from the Canton Aargau, the Swiss National Science Foundation (SNF, Grant No. 200021 1243894), the Swiss Nanoscience Institute, and the National Center of Competence in Research for Quantum Science and Technology.

-
- [1] L. Ciobanu, D. A. Seeber, and C. H. Pennington, *J. Magn. Reson.* **158**, 178 (2002).
 - [2] M. Poggio and C. L. Degen, *Nanotechnology* **21**, 342001 (2010).
 - [3] C. L. Degen, M. Poggio, H. J. Mamin, C. T. Rettner, and D. Rugar, *Proc. Nat. Acad. Sci. USA* **106**, 1313 (2009).
 - [4] R. Verhagen, A. Wittlin, C. W. Hilbers, H. van Kempen, and A. P. M. Kentgens, *J. Am. Chem. Soc.* **124**, 1588 (2002).
 - [5] K. R. Thurber, L. E. Harrell, R. Fainchtein, and D. D. Smith, *Appl. Phys. Lett.* **80**, 1794-1796

- (2002).
- [6] K. R. Thurber, L. E. Harrell, and D. D. Smith, *J. Magn. Reson.* **162**, 336-340 (2003).
 - [7] S. R. Garner, S. Kuehn, J. M. Dawlaty, N. E. Jenkins, J. A. Marohn, *Appl. Phys. Lett.* **84**, 5091 (2004).
 - [8] H. J. Mamin, R. Budakian, B. W. Chui, and D. Rugar, *Phys. Rev. Lett.* **91**, 207604 (2003).
 - [9] H. J. Mamin, R. Budakian, B. W. Chui, and D. Rugar, *Phys. Rev. B* **72**, 024413 (2005).
 - [10] M. Poggio, C. L. Degen, C. T. Rettner, H. J. Mamin, and D. Rugar, *Appl. Phys. Lett.* **90**, 263111 (2007).
 - [11] C. L. Degen, M. Poggio, H. J. Mamin and D. Rugar, *Phys. Rev. Lett.* **99**, 250601 (2007).
 - [12] C. L. Degen, M. Poggio, H. J. Mamin and D. Rugar, *Phys. Rev. Lett.* **100**, 137601 (2008).
 - [13] M. Poggio, H. J. Mamin, C. L. Degen, M. H. Sherwood, and D. Rugar, *Phys. Rev. Lett.* **102**, 087604 (2009).
 - [14] T. H. Oosterkamp, M. Poggio, C. L. Degen, H. J. Mamin, and D. Rugar, *Appl. Phys. Lett.* **96**, 083107 (2010).
 - [15] H. J. Mamin, T. H. Oosterkamp, M. Poggio, C. L. Degen, C. T. Rettner and D. Rugar, *Nano Letters* **9**, 3020 (2009).
 - [16] C. P. Slichter, *Principles of Magnetic Resonance* (Springer, Berlin, 1990), 3rd ed.
 - [17] B. W. Chui, Y. Hishinuma, R. Budakian, H. J. Mamin, T. W. Kenny, and D. Rugar, *TRANSDUCERS, 12th International Conference on Solid-State Sensors, Actuators and Microsystems* **2**, 1120 (2003).
 - [18] B. C. Stipe, H. J. Mamin, T. D. Stowe, T. W. Kenny, and D. Rugar, *Phys. Rev. Lett.* **87**, 096801 (2001).
 - [19] S. Kuehn, R. F. Loring, and J. A. Marohn, *Phys. Rev. Lett.* **96**, 156103 (2006).
 - [20] J. L. Garbini, K. J. Bruland, W. M. Dougherty, and J. A. Sidles, *J. Appl. Phys.* **80**, 1951 (1996); K. J. Bruland, J. L. Garbini, W. M. Dougherty, and J. A. Sidles, *J. Appl. Phys.* **80**, 1959 (1996).
 - [21] E. Van Veenendaal, B. H. Meier, and A. P. M. Kentgens, *Mol. Phys.* **93**, 195 (1998).
 - [22] P. T. Callaghan, *Principles of Nuclear Magnetic Resonance Microscopy* (Oxford University Press, Oxford, 1991), p. 174.
 - [23] Fei Xue, P. Peddibhotla, M. Montinaro, D. P. Weber, and M. Poggio, *Appl. Phys. Lett.* **98**, 163103 (2011).

- [24] D. J. Guerrier and R. T. Harley, *Appl. Phys. Lett.* **70**, 1739 (1997).
- [25] M. Poggio and D. D. Awschalom, *Appl. Phys. Lett.* **86**, 182103 (2005).